BOUNDS FOR AIRCRAFT TRACKING USING A HYDROPHONE ARRAY

F. Rice, D. A. Gray

CRC for Sensor Signal and Information Processing

Dept of Electrical and Electronic Engineering

Adelaide University, Australia 5005

feng,dgray@eleceng.adelaide.edu.au

I. S. D. Solomon

Maritime Operation Division

Defence Science and Technology Organisation

Edinburgh, Australia, 5108

daniel.solomon@dsto.defence.gov.au

Abstract – *Cramér-Rao lower bounds (CRLBs) for aircraft track estimates using an array of hydrophones are presented. Tracking using both bearing and Doppler frequency measurements and in a two layer (air-sea) acoustic environment are considered. The CRLBs for both bearing and Doppler frequency estimation are employed in the tracking CRLBs derivation. The CRLBs provide useful theoretic performance limits that capture the problem complexity and are independent of any particular algorithm. The CRLB gives the lower bound on errors of the estimated tracking parameters, such as the aircraft's location and velocities. The bounds also can be used to investigate how the system performance varies with typical design parameters, such as number of receivers, the operating frequency and the aircraft flight path relative to the array and the SNR of the received signal.*

Keywords: Cramér-Rao lower bounds, target tracking,nonlinear filter, hydrophone array, bearing and Doppler frequency measurements

1. INTRODUCTION

Sonar tracking with both bearing and Doppler measurements has received some attention in the literature, however most research has considered the acoustic source to be in the same plane as the sensor array, so the target tracking is pursued in two-dimensions. Here we consider the case where the source is at a different height and in a different physical medium to the sensor array. Aircraft tracking using an undersea hydrophone array [2, 8] is an example of such a challenging problem since there are two media, i.e., the acoustic energy radiated by a moving aircraft is transmitted through the atmosphere, across the air-water interface and then through the water before received by the hydrophone array.

The paper is organized into seven sections. Section 2 introduces the posterior Cramér-Rao Lower Bounds for target state estimation and the state space model used. In most cases of practical interest, the coordinates and velocity of the air-sea intercept point can be used to approximate the state vector of the aircraft. This approximation is derived in Section 3. In Section 4 the problem of obtaining generic expressions for the bearing and Doppler measurements is addressed by using CRLBs of the bearing and frequency estimates. Section 5 derives the CRLBs of two propagation media by considering a Jacobian parameter transformation in three-dimensions. Section 6 presents the comparison of the EKF performance with the new CRLBs to verify the bounds. Conclusions are given in Section 7.

In this paper it is assumed that each of the two layers is isotropic; bearing and frequency measurements are uncorrelated; there are no measurement biases for both bearing and frequency; the target speed is less than sound speed; the probability of detection $P_d = 1$ i.e., there are no false alarms nor missed detections $P_{fa} = 0$; there are N sensors used in an array; the array is linear and so only provides an estimate of the cone angle of arrival; the source emits a single stable frequency.

2. CRAMÉR-RAO BOUNDS FOR TARGET STATE ESTIMATION

Assume at time t_k, the target is located at coordinates (x_k, y_k, z_k) and moves with a nearly constant velocity vector (v_{x_k}, v_{y_k}). Consider the following linear dynamical system,

$$S_{k+1} = FS_k + W_k \tag{1}$$

where $S_k = [x_k \quad v_{x_k} \quad y_k \quad v_{y_k}]'$ is the target state at time k, and $\{W_k\}$ is a vector white noise sequence. Since neither bearing nor Doppler frequency can efficiently measure changes in the z direction, the aircraft altitude is not included in the state vector and is assumed to be a known constant.

Assuming the target flies with a nearly constant velocity (CV), F is given by [1]

$$F = \begin{bmatrix} 1 & T & 0 & 0 \\ 0 & 1 & 0 & 0 \\ 0 & 0 & 1 & T \\ 0 & 0 & 0 & 1 \end{bmatrix} \tag{2}$$

and the process noise, W_k, has covariance

$$Q_k = q \cdot \begin{bmatrix} \frac{T^3}{3} & \frac{T^2}{2} & 0 & 0 \\ \frac{T^2}{2} & T & 0 & 0 \\ 0 & 0 & \frac{T^3}{3} & \frac{T^2}{2} \\ 0 & 0 & \frac{T^2}{2} & T \end{bmatrix} \tag{3}$$

where T is the sampling interval $T = t_{k+1} - t_k$ and q is the power spectral density of the corresponding continuous time process noise [1, Section 6.2.2].

At time k, the array outputs are processed in both the spatial and temporal domains to give estimates (measurements) of the arrival direction and frequency of a narrowband signal emitted by the aircraft. Typical processing would be spectrum analysis and beamforming however, detailed discussion of these is beyond the scope of the paper. Thus at the time t_k, the measurement vector is $Z_k = [\beta_k, f_k]'$ plus random noise. The bearing, β_k, is the cone angle at which plane wave energy from the aircraft is incident upon the array and f_k is the Doppler shifted frequency of the plane wave. The estimation error for each component is discussed in Section 4.

We seek the CRLB for unbiased estimators $\hat{S}_k$ of the target state S_k, given the available sensor measurements,

$$\{Z_1, Z_2, \ldots, Z_k\}$$

The posterior Cramér-Rao bounds for target state estimation were derived by Tichavsky *et al* [9] and the following Riccati-like recursion gives the sequence of Fisher Information Matrices, J_k, for the linear dynamical system the unbiased estimation of S_k [3]:

$$J_{k+1} = \left(Q_k + F_k J_k^{-1} F_k'\right)^{-1} + J_{Z_{k+1}} \qquad (4)$$

The matrix $J_{Z_{k+1}}$ incorporates the dependency of the CRLB on the measurement model and is discussed in Section 4. The recursion in Eqn (4) requires an initial FIM, J_0, which is based on the prior distribution of the target state $p(S_0)$. If the prior distribution is Gaussian with covariance C_0, then $J_0 = C_0^{-1}$.

3. AIR-SEA INTERCEPT POINT

In this paper the time-varying bearing and Doppler frequency obtained from the outputs of a linear array of hydrophones are considered for target motion in the three dimensional plane. Assume that a sensor array is located at the origin of the coordinates, is linear along the y-axis and is at d m depth in the sea as illustrated in Fig. 1.

3.1. Target position and air-sea intercept point

Sound waves are emitted from the aircraft and refracted at the air-sea interface. The incident wavefront is picked up by each of the hydrophones in the array and are coherently processed to compute the time-varying bearing and Doppler frequency of the signal. Since the array measures both bearing and Doppler frequency of the air-sea intercept point, the locus and the velocity of the air-sea intercept point are crucial in deriving the bounds. There is no guarantee that an aircraft moving at a constant velocity will result in an intercept point doing the same. Here we investigate the relationship between the trajectory and velocity of the aircraft and the trajectory and velocity of the air-sea intercept point. For the immediate problem of interest the state is the intercept point and its velocity components i.e., $S_{ik} = [x_{ik} \quad v_{x_{ik}} \quad y_{ik} \quad v_{y_{ik}}]$. However, since the problem is formulated in terms of the aircraft positions and velocities it becomes necessary to relate the velocity and locus of the aircraft trajectory to those of the intercept point.

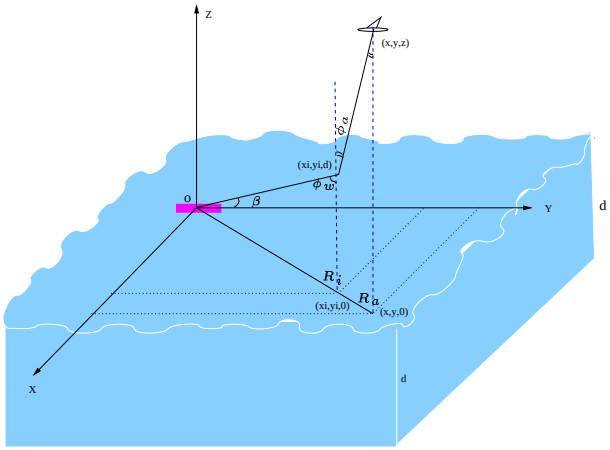

Fig. 1. 3D Geometry of source and sensors

To find the relationship between the target state $[x_k, v_{x_k}, y_k, v_{y_k}]$ and the state of the air-sea intercept point $[x_{ik}, v_{x_{ik}}, y_{ik}, v_{y_{ik}}]$, the geometry of the source and the array need be considered. This is illustrated in Figs. 1 and 2. For simplicity, the time index k has been dropped.

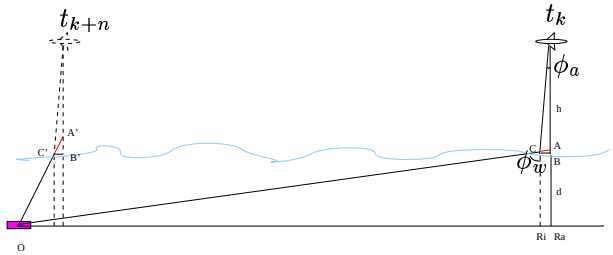

Fig. 2. Cross section

From Fig. 2 we have

$$\sin\phi_a = \frac{BC}{\sqrt{h^2 + BC^2}},$$

$$\sin\phi_w = \frac{R_i}{\sqrt{R_i^2 + d^2}},$$

where ϕ_a and ϕ_w are the incident angles with respect to the normal as indicated in Figs. 1 and 2; R_i is the range in the horizontal plane of the intercept point from the array; R_a is the target range in the horizontal plane.

From Snell's Law,

$$\frac{\sin\phi_a}{\sin\phi_w} = \frac{c_a}{c_w} = \gamma,$$

where γ is the ratio of the refractive indexes, c_a is the speed of the sound in air and c_w is the speed of the sound in the sea.

Thus we have

$$\frac{BC}{\sqrt{h^2 + BC^2}} = \gamma \frac{R_i}{\sqrt{R_i^2 + d^2}}$$

Substituting

$$BC = R_a - R_i$$

in the above equation gives

$$(R_a - R_i)^2(R_i^2 + d^2) = \gamma^2 R_i^2 \left[h^2 + (R_a - R_i)^2\right]$$

Re-arranging the above equation we obtain the following polynomial equation,

$$\begin{aligned}&(1-\gamma^2)R_i^4 - 2(1-\gamma^2)R_a R_i^3 \\ &+ \left[d^2 - h^2\gamma^2 + (1-\gamma^2)R_a^2\right] R_i^2 - 2d^2 R_a R_i \\ &+ R_a^2 d^2 = 0 \end{aligned} \quad (5)$$

for R_i.

Whilst it is difficult to solve Eqn (5) analytically, a numerical solution (by Matlab) is feasible, and is plotted in Fig. 3 together with R_a. We assume that the fixed parameters are: altitude h is 200 m, array depth d is 100 m, the aircraft flies along a straight line parallel to the array for 200 seconds at constant velocity 165 m/sec toward the array location.

Figure 3 also shows the solution for R_i as a function of y position when the aircraft flies at a constant velocity $(0, -165)$ m/s along the y-axis. Figure 4 plots the difference between R_{a_k} and R_{i_k} as a function of y position of the aircraft.

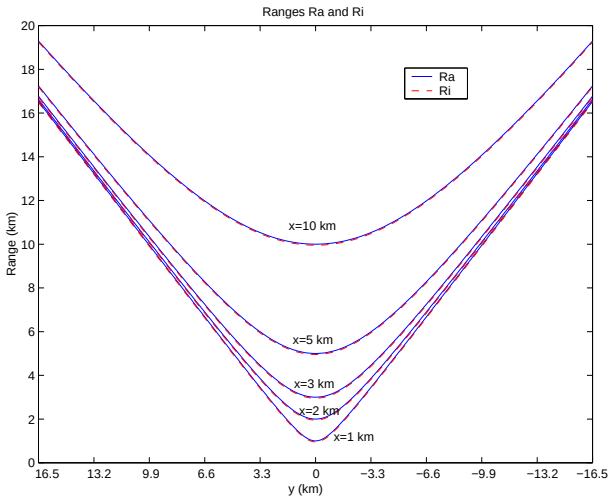

Fig. 3. Numerical solution for R_i

Figure 4 reveals that the difference between R_a and R_i is nearly constant for a fixed h. If the altitude $h = 200m$ the difference is about 46 meters. At the closest point of approach (CPA) R_i is slightly closer to R_a. Therefore, we conjecture that the radiated sound enters the air-sea interface with almost vertical angle, i.e., $\phi_a \approx 0$ [2], the trajectories of the target and the air-sea interface are approximately parallel with the only difference being the altitude h in the z direction.

To obtain the analytical relationships between the target state and the interface state the following approximation is

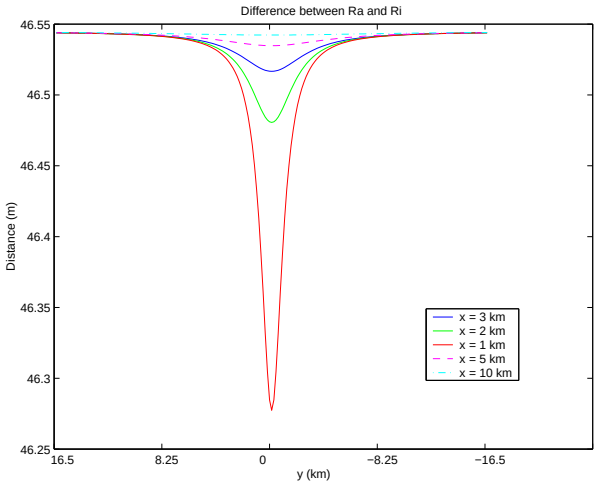

Fig. 4. True difference between R_a and R_i

made. From ΔABC,

$$\begin{aligned} AC &= \frac{BC}{\sin\phi_w} = \frac{h\tan\phi_a}{\sin\phi_w} \\ &= \frac{h\sin\phi_a}{\sin\phi_w\cos\phi_a} \approx h\gamma \end{aligned} \quad (6)$$

since $\phi_a \approx 0$.

When the target is far away in range from the array AC is approximately equal to BC. So

$$R_a - R_i = BC \approx h\gamma, \quad (7)$$

indicating that the difference between R_a and R_i is the function of the target altitude h and γ only.

From Fig.1 we have

$$R_a^2 = x^2 + y^2, \qquad R_i^2 = x_i^2 + y_i^2$$

Thus

$$\sqrt{x_i^2 + y_i^2} = \sqrt{x^2 + y^2} - h\gamma \quad (8)$$

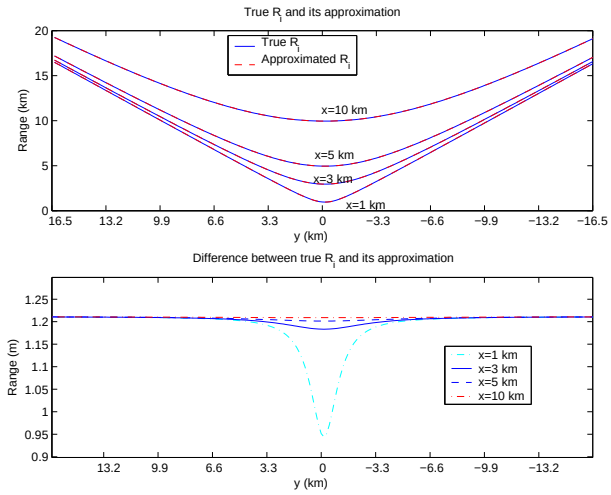

Fig. 5. True R_i and its approximation

Figure 5 shows that the approximation of R_i Eqn (8) is very close to the true value of R_i. The difference between the true R_i and its approximation is less than 1.22 m with slight nonlinear around the CPA. As x increases the difference approaches to constant value.

However, from Fig.1 we also have

$$\frac{y}{x} = \frac{y_i}{x_i}, \qquad y_i = x_i \frac{y}{x} \tag{9}$$

then

$$x_i = x\sqrt{\frac{x^2+y^2-2h\gamma\sqrt{x^2+y^2}+h^2\gamma^2}{x^2+y^2}} \tag{10}$$

and

$$y_i = y\sqrt{\frac{x^2+y^2-2h\gamma\sqrt{x^2+y^2}+h^2\gamma^2}{x^2+y^2}} \tag{11}$$

Differentiating Eqns (10) and (11) with respect to time, we obtain the velocity of the air-sea interface:

$$\frac{dx_i}{dt} = \frac{\partial x_i}{\partial x}\frac{dx}{dt} + \frac{\partial x_i}{\partial y}\frac{dy}{dt}$$
$$\frac{dy_i}{dt} = \frac{\partial y_i}{\partial x}\frac{dx}{dt} + \frac{\partial y_i}{\partial y}\frac{dy}{dt}$$

Maple^{TM} V was employed to carry out the following calculation.

$$\begin{aligned} v_{xi} &= \frac{x^4+2\,x^2\,y^2-h\,\gamma\,x^2\,\sqrt{R_a^2}}{\sqrt{R_a^2-2\,h\,\gamma\,\sqrt{R_a^2}+h^2\,\gamma^2}\,R_a^3}\,v_x \\ &+ \frac{y^2\,h^2\,\gamma^2-2\,h\,\gamma\,y^2\,\sqrt{R_a^2}+y^4}{\sqrt{R_a^2-2\,h\,\gamma\,\sqrt{R_a^2}+h^2\,\gamma^2}\,R_a^3}\,v_x \\ &+ \frac{x\,y\,h\,\gamma\,(R_a^2-h\,\gamma\,\sqrt{R_a^2})}{\sqrt{R_a^2-2\,h\,r\,\sqrt{R_a^2}+h^2\,\gamma^2}\,R_a^4}\,v_y \end{aligned} \tag{12}$$

$$\begin{aligned} v_{yi} &= \frac{x^4+2\,x^2\,y^2-2\,h\,\gamma\,x^2\,\sqrt{R_a^2}}{\sqrt{R_a^2-2\,h\,\gamma\,\sqrt{R_a^2}+h^2\,\gamma^2}\,R_a^3}\,v_y \\ &+ \frac{x^2\,h^2\,\gamma^2-h\,\gamma\,y^2\,\sqrt{R_a^2}+y^4}{\sqrt{R_a^2-2\,h\,\gamma\,\sqrt{R_a^2}+h^2\,\gamma^2}\,R_a^3}\,v_y \\ &+ \frac{x\,y\,h\,\gamma\,(R_a^2-h\,\gamma\,\sqrt{R_a^2})}{\sqrt{R_a^2-2\,h\,\gamma\,\sqrt{R_a^2}+h^2\,\gamma^2}\,R_a^4}\,v_x \end{aligned} \tag{13}$$

Figure 7 shows the velocity of the air-sea intercept point with the different x.

The air-sea interface trajectory and velocity are functions of the target state $[x_k, v_{x_k}, y_k, v_{y_k}]$, the target altitude h and the refractive index γ. Figure 6 shows a comparison of the trajectories of the target and the air-sea interface at the initial points at $(3, 16.5)$ km, $(5, 16.5)$ km and $(10, 16.5)$ km with a constant velocity of (0,-165) m/s.

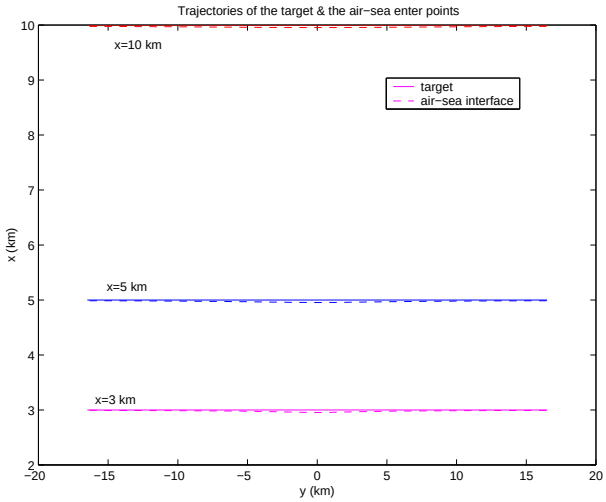

Fig. 6. Comparison of (x_k, y_k) and (x_{ik}, y_{ik}) with different x

The plots reveal that *both the locus of the intercept point and the velocity of the intercept point are approximately equal to the locus and velocity of the target respectively in horizontal plane except around the CPA.*

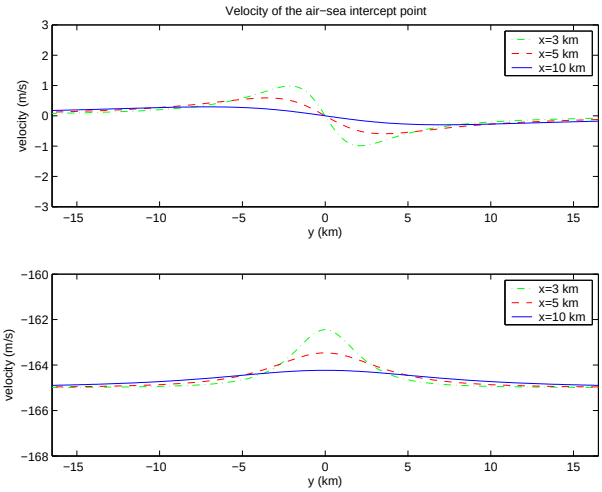

Fig. 7. Comparison of v_{xi} and v_{yi} with different x

As the plots indicate, around CPA, approximation errors of up to a maximum of 1-2 meters in position and 1-3 meters/sec in speeds occur. These will give rise to slight deviations from the constant speed state model assumed for the intercept point. However such deviations can easily be tracked by using a suitable level of process noise. Thus for all of the aircraft's trajectory its state can be well approximated by that of the air-sea intercept point moving at a constant y speed.

4. DERIVATION OF FIM

Since the velocity of the air-sea intercept point is approximately constant the CV dynamical model can be applied.

The dynamical state is

$$S_{ik} = [x_{ik} \quad v_{x_{ik}} \quad y_{ik} \quad v_{y_{ik}}]' \tag{14}$$

and can be expressed as a *linear state model*,

$$S_{i(k+1)} = FS_{ik} + W_{ik} \tag{15}$$

where W_{ik} is process noise vector with zero mean white Gaussian noise and covariance given by Eqn (3).

The target state is measured indirectly through the state of the air-sea intercept point. The measurement at the air-sea interface can be described by

$$Z_k = H_k S_{ik} + V_k$$

where H_k is the measurement matrix and V_k is a random noise vector representing measurement noise.

At time k the observer simultaneously measures the bearing β_k and the Doppler frequency f_k of the incident narrowband signal. Since the bearing is processed in temporal domain and Doppler frequency in frequency domain these two measurements can be assumed as decorrelated. From [3] the part of the measurement related FIM (Eqn (4) is given by

$$J_{Z_k} = \frac{1}{\sigma_\beta^2} E\left\{ \left[\frac{\partial \beta_k}{\partial S_k}\right]' \left[\frac{\partial \beta_k}{\partial S_k}\right] \right\} + \frac{1}{\sigma_{f_0}^2} E\left\{ \left[\frac{\partial f_k}{\partial S_k}\right]' \left[\frac{\partial f_k}{\partial S_k}\right] \right\} \tag{16}$$

where the expectation is now over the process noise.

For both bearing and Doppler frequency the actual processing algorithms, *i.e.*, beamforming and spectrum analysis, that are used to obtain the bearing and Doppler frequency estimates from the hydrophone outputs are not considered [1]. Rather it is assumed that the estimates are equal to the true values plus additive measurement noise. This approach, while producing a coarser understanding of system behavior has the advantage of not needing the specification of the exact algorithm used in the estimation process. However, it is important to be able to trace back the values used for the measurement noise powers to actual physical quantities like SNR, the number of receivers, the frequency resolution etc. To do this without considering the specification of the estimation algorithm presented a problem - this was overcome by using expressions for the variances derived from the CRLB for bearing and Doppler frequency estimates. The given results are "estimation algorithm" independent but are optimistic in these sense that they use lower bounds.

The CRLB for the intercept point is calculated using Eqn (4) and the key term to consider is J_{Z_k}. Again reference [3], see Eqn (16), allows J_{Z_k} to be evaluated using an expectation over process noise and the key quantities to be estimated are $\frac{\partial \beta_k}{\partial S_k}$ and $\frac{\partial f_k}{\partial S_k}$.

[1] As an example the bearing of a narrowband source could be estimated by using narrowband beam powers and either picking the bearing as the direction of the beam with maximum power or by using the two beams either side of it and a quadratic interpolation algorithm. The statistics of these two estimates will be quite different.

As discussed in [7, 3] it is usually not possible to evaluate Eqn (16) analytically and it is evaluated by Monte Carlo simulation.

4.1. Bearing; Linearisation and Estimation Noise

Using 3D geometry it can be shown that β, the cone angle, is given by the following, where again the time index k is omitted for convenience,

$$\beta = \arctan \frac{\sqrt{x_i^2 + d^2}}{y_i} \tag{17}$$

Thus

$$\frac{\partial \beta}{\partial x_i} = \frac{x_i y_i}{\sqrt{x_i^2 + d^2}(x_i^2 + y_i^2 + d^2)} \tag{18}$$

$$\frac{\partial \beta}{\partial y_i} = -\frac{\sqrt{x_i^2 + d^2}}{x_i^2 + y_i^2 + d^2} \tag{19}$$

and

$$\frac{\partial \beta}{\partial v_{x_i}} = 0, \qquad \frac{\partial \beta}{\partial v_{y_i}} = 0,$$

Therefore,

$$\frac{\partial \beta}{\partial S_i} = \left[\begin{array}{cccc} \frac{x_i y_i}{\sqrt{x_i^2+d^2}(x_i^2+y_i^2+d^2)} & 0 & -\frac{\sqrt{x_i^2+d^2}}{x_i^2+y_i^2+d^2} & 0 \end{array} \right]'$$

From [4], for a linear array of N equispaced sensors the CRLB for the variance of the bearing errors is given by

$$\sigma^2_{CRLB_\beta} \approx \frac{12}{4\pi^2 N \mathrm{SNR} (\frac{\mathrm{L}}{\lambda})^2 \sin^2 \beta_\mathrm{k}} \tag{20}$$

where L is the length of the array, $\lambda = c/f_0$ is the wavelength of the propagating plane wave, SNR is the signal to noise ratio at a single receiver and β_k is the time-varying cone angle. The benefit of using this expression is that it allows the performance to be evaluated as a function of typical sonar engineering design parameters.

4.2. Doppler Shift; Linearisation and Estimation Noise

Consider a signal emitted from the air-sea interface at time t_e and received by the array at time t. Thus we have

$$t = t_e + \frac{R_w(t_e)}{c_w} \tag{21}$$

where $R_w(t_e)$ is the distance between the array phase center and the air-sea interface point at time t_e. The phase of the received signal at time t is given by

$$\omega_r(t) = 2\pi f_0 t_e$$

and hence the Doppler shifted frequency at sampled time t_k is given by

$$\begin{aligned} f_{ik} = f(t_k) &= f_0 \frac{dt_e}{dt}|_{t=t_k} \\ &= f_0 \left(1 - \frac{1}{c_w} \frac{dR_w(t_e)}{dt}|_{t=t_k}\right) \end{aligned}$$

However $R_w(t_e)$ is related to the state variables by

$$R_w(t_e) = \sqrt{x_i^2(t_e) + y_i^2(t_e) + d^2}$$

and

$$\frac{dR_w(t_e)}{dt}|_{t=t_k} = \frac{x_{ik}v_{x_{ik}} + y_{ik}v_{y_{ik}}}{\sqrt{x_{ik}^2 + y_{ik}^2 + d^2}}$$

Thus, at the air-water interface,

$$f_{ik} = f_0 \left(1 - \frac{x_{ik}v_{x_{ik}} + y_{ik}v_{y_{ik}}}{c_w\sqrt{x_{ik}^2 + y_{ik}^2 + d^2}}\right) \tag{22}$$

The linearisation of the Doppler frequency measurement matrix was undertaken by using mathematical tool, Maple V^{TM}. Maple calculations (dropping the time index k for simplicity of notation) gives

$$\frac{\partial f_i}{\partial x_i} = \frac{f_0[-v_{x_i}(y_i^2 + d^2) + v_{y_i}x_iy_i]}{c_w\sqrt{(x_i^2 + y_i^2 + d^2)^3}} \tag{23}$$

$$\frac{\partial f_i}{\partial y_i} = \frac{f_0[v_{x_i}x_iy_i - v_{y_i}(x_i^2 + d^2)]}{c_w\sqrt{(x_i^2 + y_i^2 + d^2)^3}} \tag{24}$$

$$\frac{\partial f_i}{\partial v_{x_i}} = -\frac{f_0x_i}{c_w\sqrt{x_i^2 + y_i^2 + d^2}} \tag{25}$$

$$\frac{\partial f_i}{\partial v_{y_i}} = -\frac{f_0y_i}{c_w\sqrt{x_i^2 + y_i^2 + d^2}} \tag{26}$$

Then,

$$\frac{\partial f_i}{\partial S_i} = \begin{bmatrix} \frac{f_0[-v_{x_i}(y_i^2 + d^2) + v_{y_i}x_iy_i]}{c_wR_w^3} & \frac{-f_0x_i}{c_wR_w} \\ \frac{f_0[v_{x_i}x_iy_i - v_{y_i}(x_i^2 + d^2)]}{c_wR_w^3} & \frac{-f_0y_i}{c_wR_w} \end{bmatrix} \tag{27}$$

From Rife and Boorstyn [6], an expression for the CRLB of the variance of frequency errors is given by

$$\sigma^2_{CRLB_{f_0}} = \frac{6}{4\pi^2N(N^2-1)\mathrm{SNR}} \tag{28}$$

where the SNR is the signal to noise ratio prior to any Fourier transforms.

5. CRLBS FOR TWO LAYERS

Once the CRLBs for the air-water interface are determined, they can be extended to the two layer case by using a Jacobian parameter transformation. From the previous sections, we have deduced the relationship between the air-water interface location (x_{ik}, y_{ik}), velocity (v_{x_i}, v_{y_i}) and the target location (x_k, y_k), velocity (v_x, v_y). Now the transformation of Jacobian parameters formula can be applied [4].

5.1. Jacobian Parameter Transformation

For simplicity, we assume that the aircraft constantly flies at h m altitude. Then the aircraft state estimate vector is 4 elements,

$$S_k = [x_k \quad v_{x_k} \quad y_k \quad v_{y_k}]' \tag{29}$$

where (x_k, y_k, h) is the aircraft position and v_{x_k}, v_{y_k} are its speeds.

The Jacobian parameter transformation is given by

$$\frac{\partial S_k}{\partial S_{ik}} = \begin{bmatrix} \frac{\partial x_k}{\partial x_{ik}} & \frac{\partial x_k}{\partial v_{x_{ik}}} & \frac{\partial x_k}{\partial y_{ik}} & \frac{\partial x_k}{\partial v_{y_{ik}}} \\ \frac{\partial v_{xk}}{\partial x_{ik}} & \frac{\partial v_{xk}}{\partial v_{x_{ik}}} & \frac{\partial v_{xk}}{\partial y_{ik}} & \frac{\partial v_{xk}}{\partial v_{y_{ik}}} \\ \frac{\partial y_k}{\partial x_{ik}} & \frac{\partial y_k}{\partial v_{x_{ik}}} & \frac{\partial y_k}{\partial y_{ik}} & \frac{\partial y_k}{\partial v_{y_{ik}}} \\ \frac{\partial v_{yk}}{\partial x_{ik}} & \frac{\partial v_{yk}}{\partial v_{x_{ik}}} & \frac{\partial v_{yk}}{\partial y_{ik}} & \frac{\partial v_{yk}}{\partial v_{y_{ik}}} \end{bmatrix} \tag{30}$$

From Eqns (8) and (9), dropping the time index k for simplicity of notation, we obtain

$$x = x_i\sqrt{\frac{{x_i}^2 + {y_i}^2 + 2\,h\,\gamma\sqrt{{x_i}^2 + {y_i}^2} + h^2\,\gamma^2}{x_i^2 + {y_i}^2}} \tag{31}$$

and

$$y = y_i\sqrt{\frac{{x_i}^2 + {y_i}^2 + 2\,h\,\gamma\sqrt{{x_i}^2 + {y_i}^2} + h^2\,\gamma^2}{x_i^2 + {y_i}^2}} \tag{32}$$

The detailed calculation of $\frac{\partial x_k}{\partial x_{ik}}, \frac{\partial x_k}{\partial y_{ik}}, \frac{\partial y_k}{\partial x_i}, \frac{\partial y_k}{\partial y_{ik}}, etc$ can be found in [5].

$$\frac{\partial x}{\partial v_{xi}} = 0, \qquad \frac{\partial x}{\partial v_{yi}} = 0$$

Therefore

$$\mathrm{var}([\hat{S}_k]_{ii}) \geq \left[\frac{\partial S_k}{\partial S_{ik}}\right]^2_{ii} J^{-1}_{k_{ii}}$$

5.2. Evaluating CRLBs

Based on Eqn (4) and the Jacobian parameter transformation Eqn (30) the CRLBs of the target states for several scenarios were calculated by Monte Carlo simulation.

The array is present at (0,0,0) and aligned along the y-axis. The fixed parameters are: altitude h is 200 m, array depth d is 100 m. We assume the aircraft flies along a straight line parallel to the array for 200 seconds at nearly constant velocity 165 m/sec and the sampling rate is 1 sample per second. Independent white Gaussian noise is added to the x and y components of the aircraft's position with process noise $q = 0.1$. The signal to noise ratios for the bearing and the Doppler frequency measurements are assumed to be 10 dB. $\sigma_r = 25$ km and $\sigma_v = 200$ m/s are used in initializing J_0. The initial state of the target is $[3000, 0, 16500, -165]$.

Figure 8 shows the calculation results. The red solid line (over written by the blue dashed line) is the CRLBs for the air-sea interface (one layer) and the blue dashed line is the CRLBs for the target (two layers).

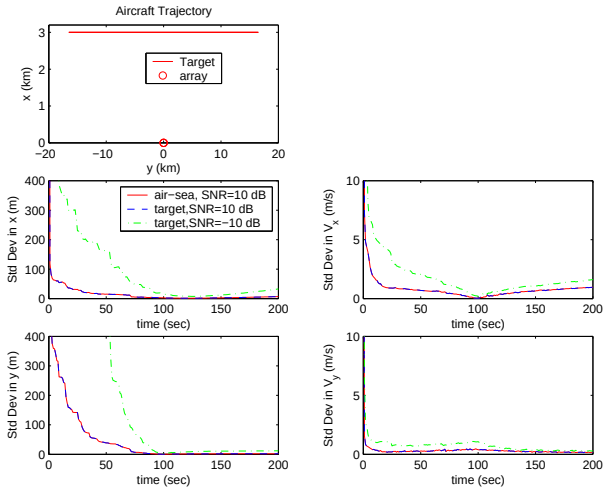

Fig. 8. CRLBs for array tracking with q=0.1 and the various measurement SNR

Figure 8 shows that the target estimation errors are less than 3 m in the y direction and 10 m in the x direction when the measurement environment SNR=10 dB. For the target velocity (v_x, v_y) the accuracy that can be achieved is about 1 meter per second. The air-sea interface results for -10 dB were also calculated have not been presented for figure clarity.

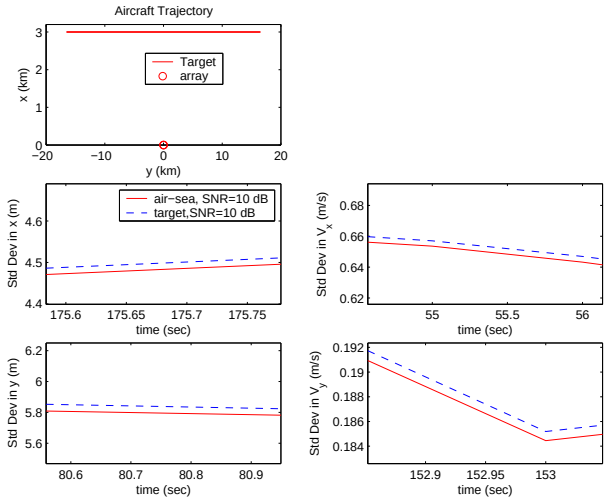

Fig. 9. Comprison of the CRLBs of one, two layers (Zoomed Figure)

There is little difference between the one layer CRLBs and the two layer CRLBs. The zoomed plot Fig.9 shows that there is less than 0.2 m difference between them with the one layer CRLBs being less than the two layer's as expected.

Since the radiated sound enters the air-sea interface with almost vertical angle, the range of the intermediate point and the velocity of the intermediate point are approximately equal to that of the target in horizontal plane (see Fig. 7) with the only difference of altitude h in the 3D domain, we conjecture that the target CRLB in horizontal plane is close to that of the air-sea intercept point. Several scenarios have been investigated and agree with the above surmise. The difference between the one layer bound and the two layer bound is less than 1 meter. Therefore, the CRLB of the air-sea intercept point can serve as a useful approximation of the target CRLB, as it is much easier to derive.

6. VERIFICATION OF THE NEW BOUNDS

The extended Kalman filter (EKF) was employed to verify the new bounds.

Section 3.1 has drawn an important conclusion that the trajectory of the intercept point and the velocity of the intercept point are approximately equal to the range and velocity of the target respectively in horizontal plane, i.e., the dynamic state $S_k = [x_k, v_{x_k}, y_k, v_{y_k}]'$ of the target is approximately equal to that of the air-sea intercept point $S_{ik} = [x_{ik}, v_{x_{ik}}, y_{ik}, v_{y_{ik}}]'$. Therefore, the target state S_k substitutes for the state of the air-sea intercept point S_{ik} in the measurement related calculation throughout the EKF procedure, which simplifies the computation significantly.

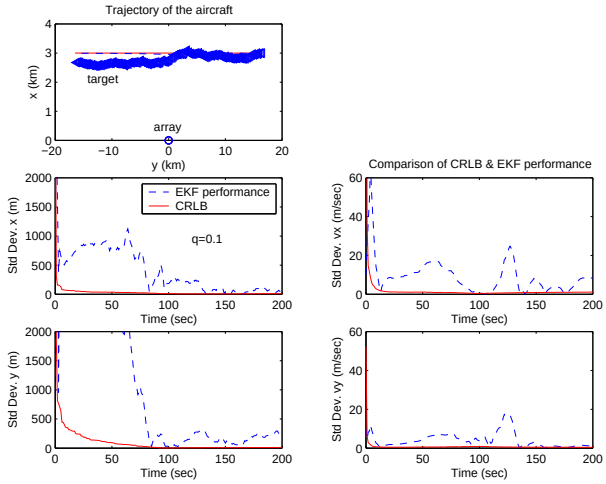

Fig. 10. EKF Performance with $\sigma_\beta = 3^0, \sigma_f = 1$ Hz

Figure 10 shows that the EKF performance when the process noise $q = 0.1$ and the measurement errors are $\sigma_\beta = 3^0, \sigma_f = 1$ Hz. The trajectory starts at $S_0 = [3000 \quad 0 \quad 16500 \quad -165]'$ and the process noise is modeled as white Gaussian with standard deviation $\sigma_x = \sigma_y = 25$ m. The initial state for the tracker is $\hat{S}_0 = [S_0(1) + 1000 \quad S_0(2) + 10 \quad S_0(3) + 1000 \quad S_0(4) + 10]'$. There are 10,000 runs in the simulation. The CRLBs of the same scenario are also plotted in the figure. The simulation results show the EKF performance is lower bounded by the CRLBs.

7. CONCLUSION

The paper has derived the Cramér-Rao lower bounds for tracking an aircraft flying at constant altitude and velocity past a linear array of hydrophones using the time-varying bearing angle and Doppler frequency as measurements. An assumption of known source frequency has been made.

This study has revealed an important finding that the range of the trajectory of the intercept point and the velocity of the intercept point are approximately equal to the range and velocity of the aircraft respectively in the horizontal plane. Therefore, using the air-sea interface state in an EFK provides a solution, which is a good estimate of the aircraft trajectory, and as a result the computation of the EKF tracker is simplified significantly.

The new bounds show that the CRLBs (standard deviation) of the air-sea intercept point are only about 0.5 meter different than that of the aircraft (two layers). The Monte Carlo simulation results have verified the new bounds and show the tracker performs reasonably well.

8. REFERENCES

[1] Y. Bar-Shalom and X. Li. *Estimation and tracking : principles, techniques, and software*. Artech House, 1993.

[2] B. G. Ferguson and K. L. Lo. Transiting aircraft parameter estimation using underwater acoustic sensor data. *IEEE Journal of Oceantic Engineering*, 24(4):424–435, Oct. 1999.

[3] M. L. Hernandez, A. D. Marrs, N. I. Gordon, S. Maskell, and C. M. Reed. Cramer-Rao bounds for non-linear filtering with measurement origin uncertainty. *Proceedings of the 5th International Conference on Informa- tion Fusion*, 1:18–25, July 2002.

[4] S.M. Kay. *Fundamentals of Statistical Signal Processing: Estimation Theory*. Prentice-Hall, Englewood Cliffs, NJ, 1993.

[5] F. Rice and D. A. Gray. *Cramer-Rao Lower Bound for Aircraft Tracking using Multiple Hydrophones, Part I: Known Rest Frequency*. CSSIP Report: CR No: 7/03, June, 2003.

[6] D. C. Rife and R. R. Boorstyn. Single-tone parameter estimation from discrete-time observations. *IEEE Trans. Inform. Theory*, IT-20(5):591–598, September 1974.

[7] B. Ristic, S. Zollo, and S. Arulampalam. Performance bounds for manoeuvring target tracking using asynchronous multi-platfoml angle-only measurements. *Proceedings of 4th Annual Conference on Informa- tion Fusion*, 2001.

[8] I.S.D. Solomon and A. J. Knight. Tracking of airborne acoustic sources using an undersea hydrophone array. *Australian Acoustical Society Conference (Acoustics 2000)*, pages 79–86, November 2000. Perth.

[9] P. Tichavsky, C. H. Muravchik, and A. Nehorai. Posterior Cramer-Rao bounds for discrete- time nonlinear filtering. *IEEE Trans. Signal Processing*, (46(5)):1386–1396, 1998.

Acknowledgements

The authors would like to acknowledge the support of Defence Science and Technology Organisation of Australia and Cooperative Research Center for Sensor Signal and Information Processing in undertaking this work